Alexandria Engineering Journal (2023) 77, 369–381

HOSTED BY

Alexandria University

Alexandria Engineering Journal

www.elsevier.com/locate/aej
www.sciencedirect.com

ORIGINAL ARTICLE

# Numerical investigation of the effect of changes in blood viscosity on parameters hemodynamic blood flow in the left coronary artery with consideration capturing fluid–solid interaction

Zahra Sadeghi Nogourani [a,*], As'ad Alizadeh [b], Hayder Mahmood Salman [c], Tariq J. Al-Musawi [d], Pooya Pasha [e,*], Muhammad Waqas [f], Davood Domiri Ganji [e]

[a] School Of Medicine, Najafabad Branch, Islamic Azad University, Najafabad, ESFAHAN, Iran
[b] Department of Civil Engineering, College of Engineering, Cihan University-Erbil, Erbil, Iraq
[c] Department of Computer Science, Al-Turath University College, Al Mansour, Baghdad, Iraq
[d] Building and Construction Techniques Engineering Department, Al-Mustaqbal University College, 51001 Hillah, Babylon, Iraq
[e] Department of mechanical Engineering Mazandaran University of science and technology, P.O. Box47166-85635, Babol, Iran
[f] NUTECH School of Applied Sciences and Humanities, National University of Technology, Islamabad, Pakistan

Received 24 December 2022; revised 2 June 2023; accepted 2 July 2023
Available online 7 July 2023

KEYWORDS

Coronary artery;
Fluid and structure interaction;
Hemodynamics of blood flow;
Wall shear stress;
Stickiness

**Abstract** Cardiovascular diseases are unfortunately one of the leading causes of death in today's society. It is important to analyze blood flow in various parts of the circulatory system. The coronary artery is made up of four main arteries, and the left coronary artery is responsible for delivering blood to the heart muscle. This research utilizes computational fluid dynamics and finite element methods to investigate and analyze coronary vessels by studying changes in blood characteristics. The aim of this study is to analyze and model the flow of blood under different conditions of the coronary vessels, with a particular focus on the vessels on the left side. This is in response to changes in hematocrit, which can cause an increase or decrease in blood viscosity ($\mu_p$) (N.s/m$^2$). In general, by applying condition flexibility for the vessel, it is possible to reduce pressure distribution on the wall when compared to the rigid model. When considering changes in viscosity ($\mu$) (kg/m. s), such as an increase from 0.0029 to 0.0067, this can lead to changes in the shear stress distribution (N/m$^2$) on the wall. Specifically, this increase in blood viscosity ($\mu_p$) (N.s/m$^2$) causes maximum tension, resulting in the wall shear WSS (N/m$^2$) rising from 60 to 154 Pascal's, which is a 140% increase. Based on the current data, it appears that there is a high flow pressure in the artery, resulting in maximum relative pressure values of 6300 and 6450 Pascal's for the rigid and flexible models, respectively, at the separating joint of the bifurcation.



* Corresponding authors.
E-mail addresses: zahra.sadeghi7341@gmail.com (Z.S. Nogourani), pasha.pooya@yahoo.com (P. Pasha).

Peer review under responsibility of Faculty of Engineering, Alexandria University.

https://doi.org/10.1016/j.aej.2023.07.003

**Nomenclature**

| | | | |
|---|---|---|---|
| CFD | **C**omputational fluid dynamics | t | **T**ime (s) |
| $U$ | **V**elocity vector (m/s) | $\rho$ | **D**ensity (kg/m$^3$) |
| Re | **R**eynolds number | μ | **D**ynamic viscosity (kg/m. s) |
| ∇ | **N**abla operator | $P$ | **P**ressure (pa) |
| $T$ | **C**auchy stress tensor (N/m$^2$) | I | **I**dentity matrix |
| $f$ | **V**olumetric force of fluid (N) | $\mu_p$ | **B**lood plasma viscosity(N.s/m$^2$) |
| $\gamma$ | **C**utting rate | $\rho_w$ | **A**rterial density |
| D | **S**train rate | $v_i^n$ | **D**isplacement vector |
| HCT | **H**ematocrit | r | **R**adius of the vessel |
| Ω | **S**olution domain | $\omega$ | **C**urrent pulse frequency |
| WSS | **W**all shear stress (N/m2) | v | **P**oisson's ratio |
| FSI | **S**tructure and fluid interaction | | |
| E | **M**odulus of elasticity | | |

## 1. Introduction

The presence of vascular diseases can result in irregular flow dynamics and increased stress on cells and plaques, which can contribute to disease complexity. Understanding the rheological behavior of blood in these circumstances is crucial for comprehending blood flow dynamics and its role the development of blood components. Until 1960, it was theorized that hemodynamics could play a role in atherosclerosis, but the theory was not yet fully formulated. Hemodynamic parameters, such as blood flow velocity, blood pressure, and wall shear stress, are directly related to the pathophysiology of vascular diseases. Therefore, it is necessary to examine the dynamic properties of the fluid and take decision-making about treatment approaches into consideration. With the remarkable progress of numerical solution methods in modeling and 3D imaging techniques, a wide range of applications for the mechanical study of the cardiovascular system according to the particular models of each patient have become possible [1]. These methods make it possible to examine the details of flow dynamics, which are of great importance in determining the health and pathology of individuals, designing medical instruments and diagnoses, and deciding on the best treatment method [2]. Hematocrit is a standard that indicates the ratio of the volume of red blood cells to the total blood volume, and it can increase blood viscosity. Red blood cells have a significant impact on blood viscosity, as they are transient and determine the rheological properties of blood. Many studies have shown the importance of blood viscosity in the physiological function of tissues and organs [3]. In a study by González and Moraga [4], two models of Casson and Newton were used in an artery without occlusion, which revealed that the shear stress index in non-Newtonian and Newtonian states differed by only 5%. Therefore, the assumption of a Newtonian fluid is acceptable for simulating blood. Silveira and his colleagues [5] conducted research to determine whether complex geometries are truly necessary. Nardi and his colleagues [6] studied the hemodynamic behavior of blood flow in the branching part of the coronary artery and the three standard treatment methods available. The results were validated using flexible and transparent laboratory models [7]. Recent research has specifically investigated the effect of vessel flexibility on hemodynamics. In other words, the interaction between vessel structure and fluid has been studied extensively in the last few years. The high flexibility of the vessel has been found to impact the flow of blood, which is why this area of study has garnered significant interest. Baresi et al. [8] investigated the interaction between the structure and fluid by narrowing the artificial duct in the flow path of the coronary arteries. In a similar study, Meza and colleagues examined the left coronary arteries by considering the interaction between the system and the fluid [9]. They caused a 7% blockage in the blood vessel, resulting in its narrowing. The researchers investigated the hemodynamics of blood flow and the mechanical behavior of the structure. As a result of the blockage, the velocity and shear stress on the wall increased. On the other hand, the tensile strain on the wall has decreased. In their research, Bukač and colleagues investigated the effect of springing on the stresses created on the wall [10], and found that it had better performance than the other three models. Roustaei et al. [11] investigated the effect of blood pressure on the mechanical behavior of the diaphragm while considering fluid interaction. They thought that the wall of different vessel layers had different mechanical properties. In new research, Qiao and colleagues [12] investigate the interaction between the vessel wall and the blood fluid. They simulated the vessel's distribution of red blood cells using the mixed multiphase model. Hosseinzadeh et al. [13] investigated the effect of including nanoparticles on blood flow near the magnetic field in a porous blood vessel. A novel technique called the Akbari-Ganji's Method (AGM) in conjunction with the differential transformation method (DTM) has been applied to address this issue. The method considers blood as a third-grade non-Newtonian fluid and assumes a constant viscosity for the nanofluid. By using mathematical analysis and data structures, the field of computational fluid dynamics (CFD) can study and resolve issues involving fluid flows. Computer computations are necessary to simulate the free-stream flow of fluids and their interactions with surfaces constrained by boundary conditions, including liquids and gases. The best results are often achieved with high-velocity supercomputers, which are frequently needed to tackle the most challenging issues [14–20]. Aerodynamics, aerospace research, hypersonic technology, weather modeling, natural science, environmental engineering, industrial process structural analysis, biological engineering, current flows, and heat exchange are just a few

examples of the numerous fields of research and industries where CFD (Computational Fluid Dynamics) is used [20–28]. Additionally, Ali and his colleagues [29–33] conducted helpful research in the field of hemodynamic blood flow through analytical and fluid methods using various nanoparticles. Several researchers have explored the topic of blood flow calculations in vessels using the fractional model and have experimented with different nanomaterials to transfer micro vascular solutes [34–40]. By extracting the simulation results and analyzing the fluid's effect on the vessel wall based on the shear stress values; we can gain a better understanding of the role of viscosity in flow characteristics [41–49]. As blood viscosity plays a significant role in the development of vascular diseases, such as coronary vessels, this research aims to investigate the impact of different viscosities, both lower and higher than usual. With the combination of computational fluid dynamics and finite element methods, this research is limited to analyzing and examining coronary vessels based on changes in blood characteristics. This article's innovation lies in its investigation and comparison of two states: the rigid and flexible wall. The research discusses changes in pressure, velocity, shear stress, and other flow and concrete variables. Additionally, all the simulations done with the finite volume method were solved for the first time for this issue. The subject of this article is crucial due to the prevalence of cardiovascular diseases in modern societies. As such, analyzing blood flow in various parts of the human body is essential. The goal of this research is to model and analyze flow in different conditions of coronary vessels, particularly the left coronary vessels, due to changes in hematocrit that can cause an increase or decrease in blood viscosity.

## 2. Problem definition

This section presents the equations governing the flow field, structure, and applied boundary conditions. The influential variables in the mechanical properties of the fluid are also displayed, with the assumption that blood is a Newtonian fluid. Additionally, numerical solution methods and discretization are briefly explained.

### 2.1. Equations governing the flow

The density of blood is approximately 1060 kg/m$^3$, and it is denser than water due to the accumulation of red blood cells. The formula for calculating blood density is as follows [28]:

$$\rho \frac{\partial u}{\partial t} + \rho(u.\nabla)u = divT \tag{1}$$

$$divu = 0 \tag{2}$$

In these equations, 'u' represents the velocity vector, and 'ρ' represents the blood density. The Cauchy stress tensor, 'T', is calculated from the shear and vertical stresses using the following equation [28]:

$$T = -pI + 2\mu.D \tag{3}$$

P is the fluid pressure, I is the same matrix, dynamic fluid viscosity is μ, and D is the strain rate tensor can be calculated from the following equation [28]:

$$D(u) = \frac{1}{2}\left(\nabla u + \nabla u^2\right) \tag{4}$$

### 2.2. Properties of blood

The density of blood is approximately 1060 kg per cubic meter, which is due to the accumulation of red blood cells. To calculate blood density, you can use the following formula:

$$\rho = 1026 + (67 \times HCT(\%)) \tag{5}$$

Hematocrit (Hct) refers to the volume percentage of red blood cells in blood density. In this research, we have considered blood density to be constant and equal to 1060 kg/m$^3$ in all simulations, in order to better understand the effect of viscosity. Although blood viscosity is strongly dependent on temperature, the constant temperature of the body ensures that blood temperature remains constant. However, blood viscosity is subject to changes based on parameters such as hematocrit, shear rate, and even duct diameter. Although we can ignore the effects of shear rate on blood when considering its Newtonian behavior, there is a strong correlation between blood viscosity and hematocrit, as expressed in equation (6):

$$\mu_\infty = \mu_p[1 + 0.025H_t + 7.35 \times 10^{-4}H_t^2] \tag{6}$$

Fig. 1 illustrates the changes in blood viscosity for varying hematocrit values. As observed in the figure, viscosity values increase or decrease with an increase or decrease in hematocrit. This study examined the impact of five distinct blood viscosities, which are listed in (Table 1):

Table 1 displays the changes in blood viscosity across different states of the human body and vessels. As the condition becomes more critical, the viscosity of the blood increases from the normal level.

### 2.3. Finite element method

The finite element method is a numerical technique that can be used to solve various engineering problems in different steady, transient, linear, or nonlinear states. The method revolutionized the industry and the world by creating a new way of looking at design and analysis. The finite element method solves the

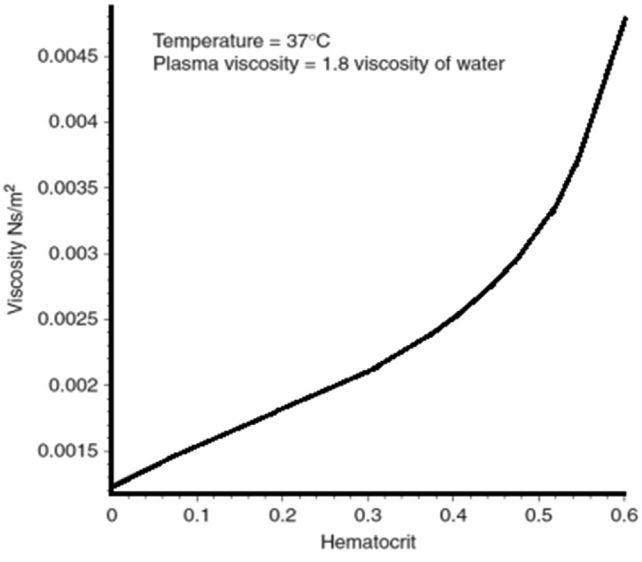


**Fig. 1** Showing changes in blood viscosity according to different hematocrit values [45].

**Table 1** Different states of blood viscosity.

| Condition | Viscosity | Number |
|---|---|---|
| Conditions below normal | 0.00289 | 1 |
| Natural conditions | 0.003511 | 2 |
| More than normal conditions | 0.004909 | 3 |
| Close to crisis | 0.006877 | 4 |
| critical | 0.009241 | 5 |

differential equations for each element by considering interpolation functions and governing equations extracted from a component. The governing equations for the entire model are obtained by combining the equations of each element. Eventually, the differential equations governing the entire model are replaced by either linear or non-linear algebraic equations. The finite element method is used for the following reasons:

- Ability to model real industrial processes
- Ability of the method to provide reliable results and...

### 2.4. The geometry of the problem

The movement of the artery wall will be determined by solving the following equation:

$$\rho_{wj} v_{i,n} = \sigma_{i,j}, i,j = 1,2,3 \tag{7}$$

Since there is no force acting on the outer wall of the artery:

$$\left|\sigma_{ij}.n_j\right| = 0 \tag{8}$$

That $\rho_{wj}$ is the arterial density, $v_{in}$ is the displacement vector, and $\sigma_{ij}$ is the stress tensor.

The study conducted in this research is on the left coronary artery. We created this geometry using Katia software (Fig. 2), and the dimensions of the artery are presented in Table 2. Additionally, we considered the thickness of the artery wall to be 0.4 mm throughout the entire domain.

### 2.5. Model networking

To mesh the geometric model, we used an organized mesh, as shown in Fig. 3. The meshing process was conducted using the ICEM CFD software, which is known for its powerful grid generation capabilities. After creating the geometric model in Catia software, we imported it into ICEM CFD for meshing. We utilized an organized mesh to mesh the geometric model, as shown in Fig. 3.

Fig. 4 represents the quality of the generated mesh through a histogram that plots the number of elements against their respective quality values, ranging from zero to one on the horizontal axis. The simulation was conducted using Comsol software, employing the transient solver, and assuming a slow flow without heat transfer. Second-order accuracy methods were used for both the discretization of the momentum equation and the time discretization of the equations. Furthermore, the Piezo method was utilized for pressure and velocity coupling. To guarantee the solution's independence from the time step, simulations were conducted for time intervals of 0.001 and 0.0005 s.

At the inlet boundary, a mass flux profile was applied over time. The boundary conditions for input and output are depicted in Fig. 5, while Table 3 offers further insights into the mesh quality of the blood flow passing through the left coronary artery.

By drawing the output static pressure diagram in terms of Pascal's (Fig. 6), the minimum output pressure is 8066 Pascal.

Regarding the reference pressure, the simulation outputs two pressures - relative pressure and reference pressure:

$$P_{st} = P_{ref} + P_g \tag{9}$$

Regarding the reference pressure, the simulation outputs two pressures - relative pressure and reference pressure. This boundary condition specifies the tangential movement of nodes along the boundary and prevents any vertical movement. Within the joint fluid and structure (inner wall of the vessel), the compressive forces and shear generated by the blood flow apply pressure to the arterial structure, causing the vessel to move.

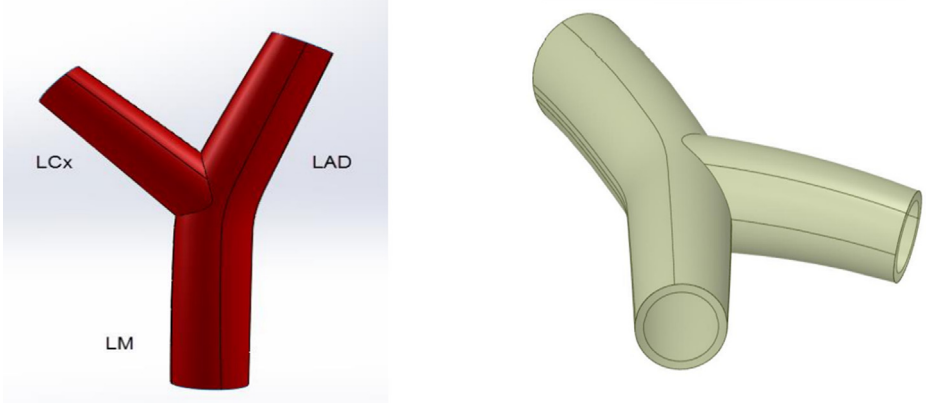


**Fig. 2** The geometry produced in Katia software.

**Table 2** The dimensions of the generated geometric model.

| 11 mm | LM length |
|---|---|
| 4 mm | LM(Left main artery) diameter |
| 3.4 mm | LAD(left anterior descending) diameter |
| 3 mm | LCX (left circumflex artery) diameter |

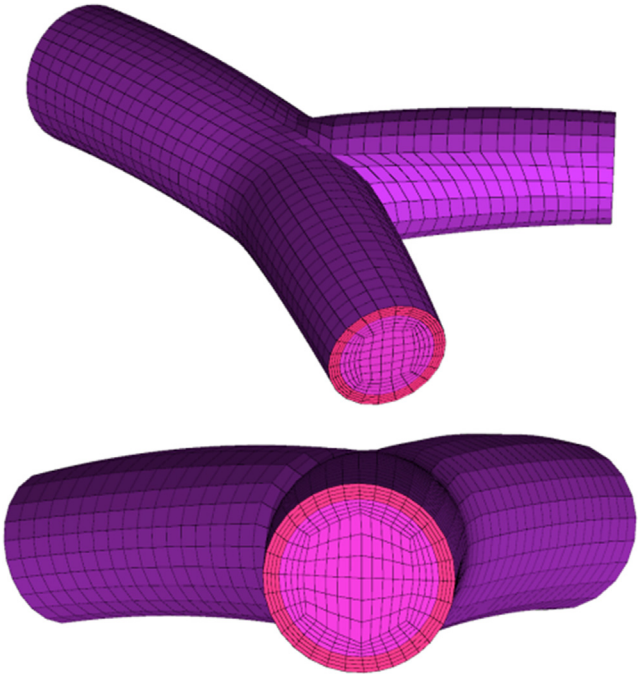

**Fig. 3** Geometry grid.

## 3. Validation

Basic fluid equations are typically non-linear and more complex than structural equations. Therefore, it is crucial to utilize an accurate model for validating the fluid solver. In this study, the fluid part was validated using a geometric model of the coronary arteries with a rigid wall. In Fig. 7, a comparison is made between the shear stress results of the current study and the research presented in [27]. Both graphs show similar trends, which assure the accuracy of the fluid solver results. Both numerical and analytical methods confirm that the initial and final points play a significant role in verifying the accuracy of the problem solutions. Based on these results, the trends of changes in both graphs are similar. This is evident from the accuracy of the solver's fluid results. The numerical and analytical methods both demonstrate that the initial and final points are crucial in verifying the accuracy of the solutions to these problems.

## 4. Results and discussion

Fig. 8 presents the maximum vessel wall deformation values in meters over time for the three networks. The results for networks 7e3 and 15e3 exhibit very similar convergence. Therefore, the 7e3 element mesh will be used as the final mesh for the rest of the simulations.

The velocity, pressure, and shear stress of the arterial wall were investigated and analyzed at three critical moments during the cardiac cycle, as shown in Fig. 9. These critical moments are as follows:

$t_1$: The moment of maximum pressure, $t_2$: The moment of maximum velocity, $t_3$: The moment of the lowest velocity.

Figs. 10, 11, and 12 depict the relative pressure distribution during a cardiac cycle for two wall models: rigid and flexible. The simulations were conducted using a viscosity of 0.0035, representing normal conditions. At the beginning of the cardiac cycle, the pressure at the entrance increases. After opening the valve in the aorta, the blood flow accelerates throughout the artery. As shown in Fig. 10, at a specific moment, the flow pressure in the artery reaches high values, with the maximum relative pressure of 6300 and 6450 Pascal for the rigid and flexible wall models, respectively, at the separating joint of the bifurcation. Furthermore, the pressure values are consistently higher on the rigid wall as compared to the flexible wall, at all times. In a flexible wall, a part of the fluid pressure is utilized to bend the wall and increase the volume of the fluid region. As the volume of the fluid region expands, the fluid pressure decreases.

As time progresses, the flow pressure in the vessel decreases. However, the pressure difference between the inlet and outlet increases until it reaches its maximum value at the moment when the flow velocity is highest (refer to Fig. 11).This process of pressure reduction continues until it reaches its lowest value at the end of the cardiac cycle. Fig. 12 illustrates that the vessel

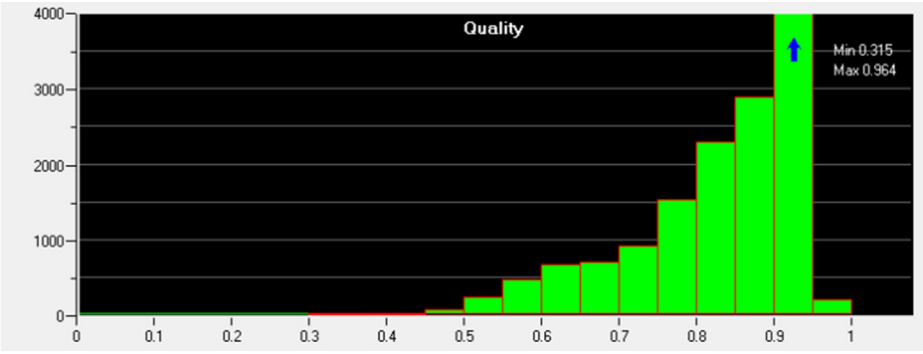


**Fig. 4** Mesh quality histogram.

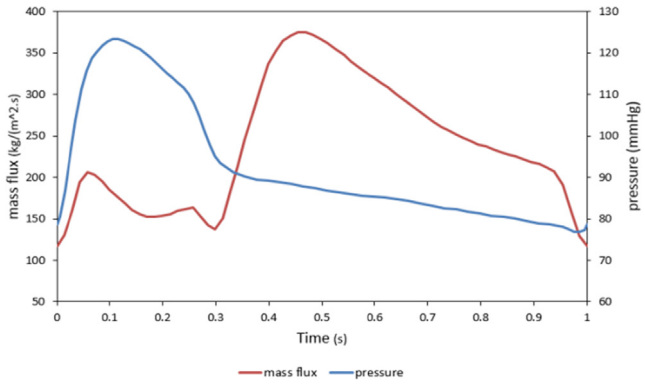


**Fig. 5** Boundary conditions of the problem; Verdi of mass flow and outputs according to pressure [28].

**Table 3** Specifications of the network related to blood flow in the left coronary artery.

| **Mesh Specifications** | |
|---|---|
| **Method:** | Patch Conforming, Tetrahedrons |
| **Body Size Type:** | Element Size |
| **Size Function:** | Curvature |
| **Quality:** | Medium |
| **Medium Mesh:** | Elements: 14,755,425<br>Nodes: 2,666,941 |

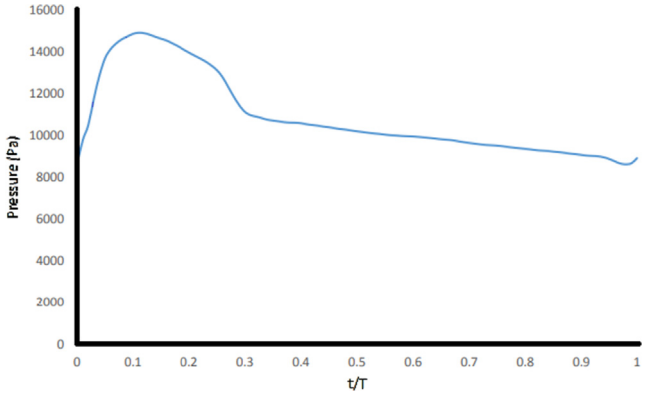


**Fig. 6** Output pressure (Pascal) according to time.

exhibits minimal pressure differences, resulting in a uniform distribution.

Fig. 13 displays the average wall pressure over time for both models. As depicted in this figure, the pressure on the rigid wall is generally higher than on the flexible wall during the cycle. For a more precise understanding of the velocity field while considering the artery wall's flexibility, Fig. 14 to Fig. 16 illustrate the velocity field for two states of the rigid and flexible wall. Fig. 14 shows the flow velocity distribution in coronary artery sections. In the rigid wall of the main branch of the vessel, the flow concentration is in the vessel's center and the flow velocity is very low near the wall. However, in high-velocity branches, the flow is diverted toward the inner walls of the

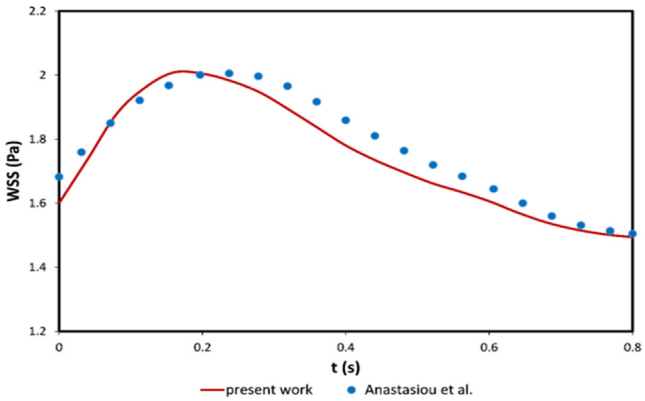


**Fig. 7** Validation of the solution method by comparing the obtained results with the experimental results of the study [27].

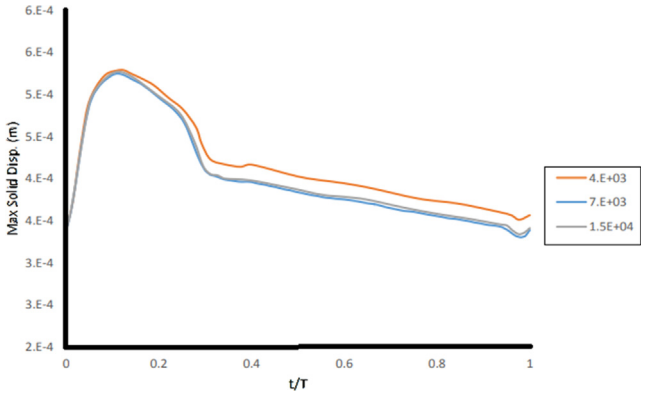


**Fig. 8** Diagram of independence from the network.

components. In contrast, the flexible wall model results in a significantly different flow field. The change in the shape of the wall will ultimately bring the flow field under the radius, causing an increase in fluid velocity near the wall. This means that the velocity of the fluid will be placed under the velocity radius of the wall, leading to an increase in velocity in its vicinity. At moment t2 for models (Fig. 15), flow movement and concentration of high flow velocities are visible. The flow velocity in the center of the artery reaches around 0.7 m/s for the rigid wall model. However, when considering the flexibility of the wall, the cross-sectional diameter of the fluid passage increases due to the application of shear and compressive stress from the fluid to the wall. As a result, compared to the rigid model with the assumption of a constant flow rate, the velocity decreases. Additionally, in the solid model, the flow velocity near the inner walls is significantly higher in the branches than in other areas. With the decrease of the input current, the flow velocity reduces, and its maximum velocity reaches around 0.3 m/s. The flow velocity distribution at this moment is depicted in Fig. 16.

Investigating the distribution of wall shear stress is extremely important as it plays a crucial role in the development and progression of cardiovascular diseases. Therefore, the distribution of this parameter during different moments of the cardiac cycle has been studied. A comparison between rigid and flexible models has been presented for shear stress. Fig. 17 displays the wall shear stress distribution for both mod-

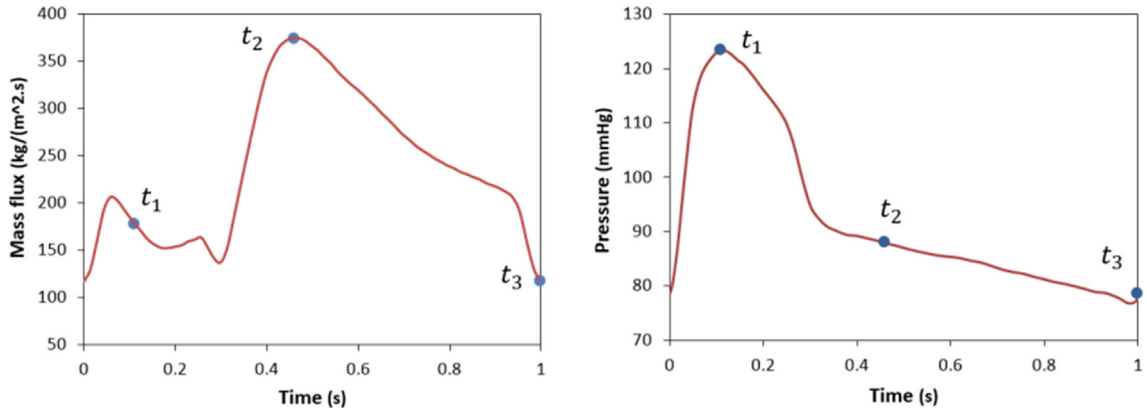


**Fig. 9** The position of critical moments in a cycle of the heart.

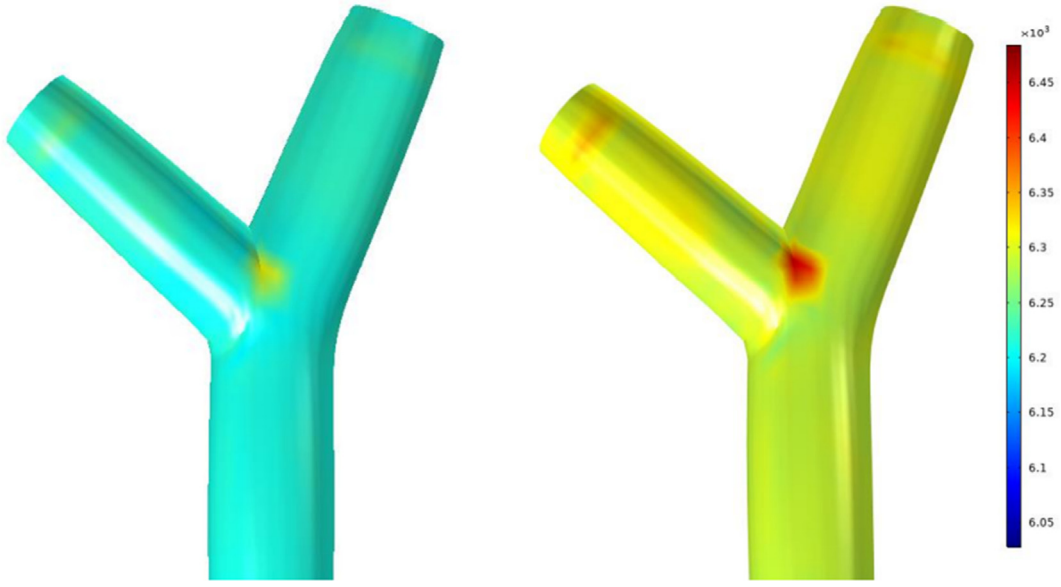


**Fig. 10** Pressure distribution at moment $t_1$ for viscosity 0.0035pa.s, right: rigid, left: flexible.

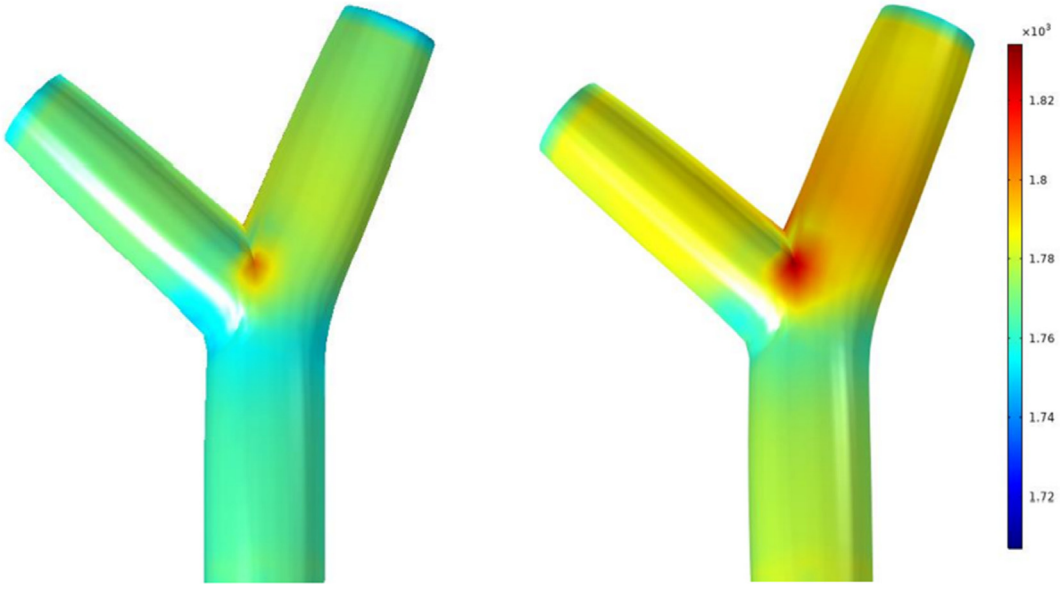


**Fig. 11** Pressure distribution at moment $t_2$ for viscosity 0.0035pa.s, right: rigid, left: flexible.

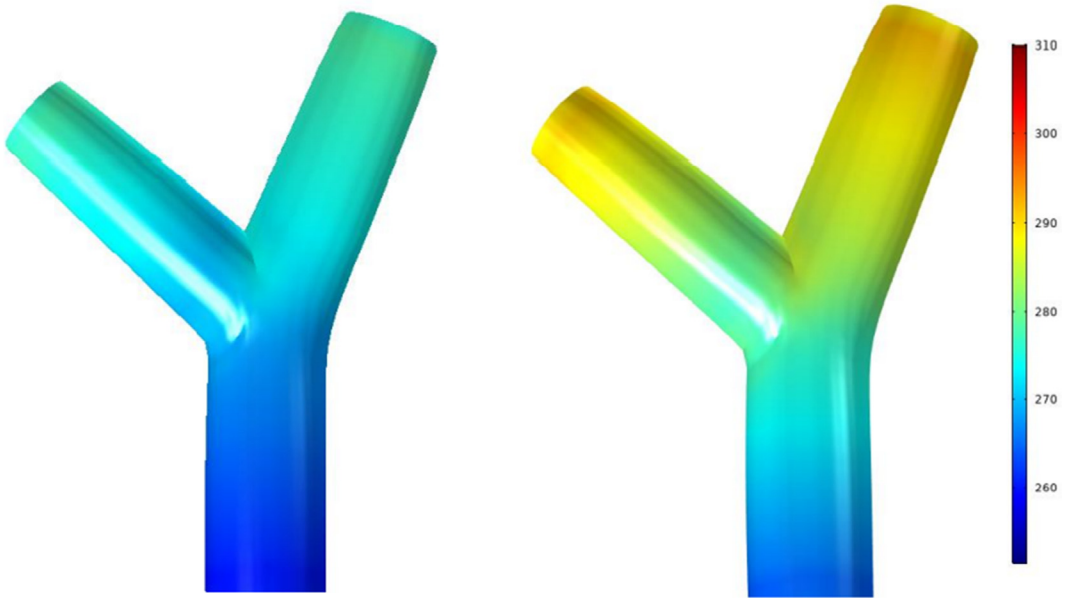


**Fig. 12** Pressure distribution at moment $t_3$ for viscosity 0.0035pa.s, right: rigid, left: flexible.

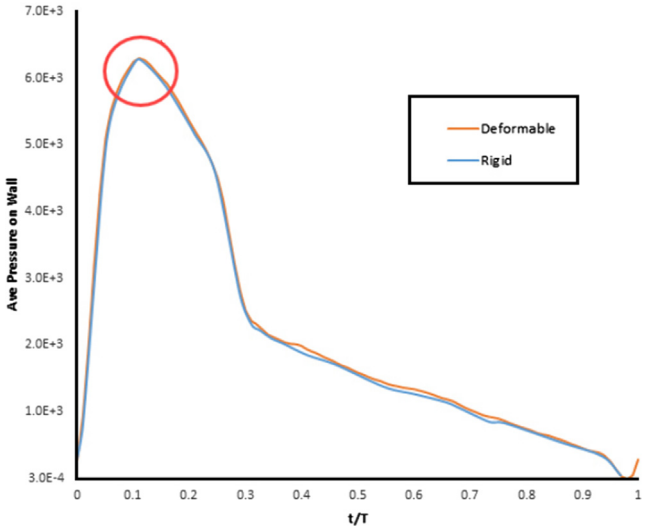


**Fig. 13** Average wall pressure in two rigid and flexible wall models.

els. In the case of the rigid model, a minimal cut has been made to the vessel wall, and only a small area of the connection displays a significant number of branches for this parameter. While in the flexible model, the septum's expansion in the bifurcation region has increased the forces between the structures and involved more areas. At the moment t2 (as shown in Fig. 18), with the increase in flow velocity, the wall's shear stress values also increase significantly. As expected, the shear stress near the inner wall of the branches has increased enormously with the increase of flow velocity. This observation confirms the direct relationship between flow velocity and wall shear stress values. In any area where the flow velocity near the wall is high, the shear stress values on the wall are significant. With the same reasoning, when the flow velocity reaches its lowest value, the shear stress values on the wall are minimized (see Fig. 19). It is worth noting that the shear stress field is similar for both the rigid and flexible models, as has been reported. However, changing the shape of the wall has caused the area of high tension to either increase or decrease.

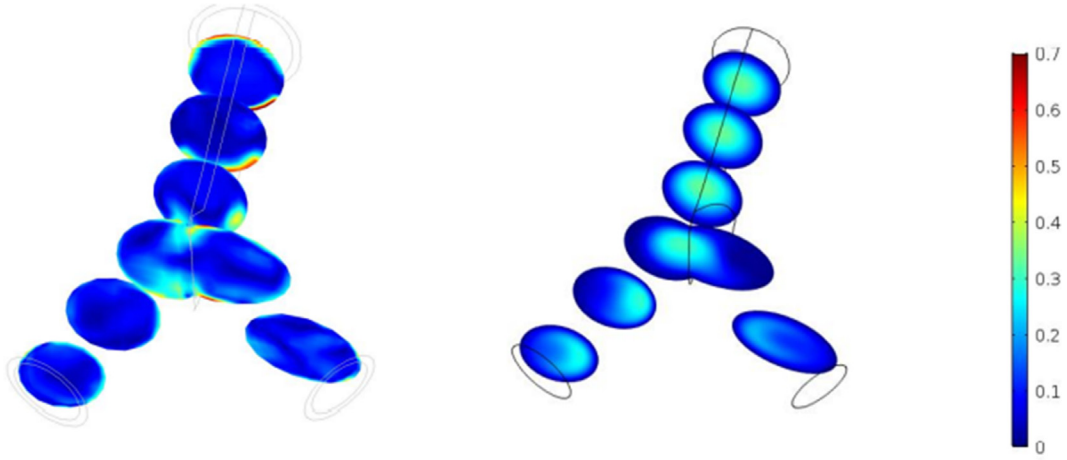


**Fig. 14** Velocity distribution at moment $t_1$ for viscosity 0.0035pa.s, right: rigid, left: flexible.

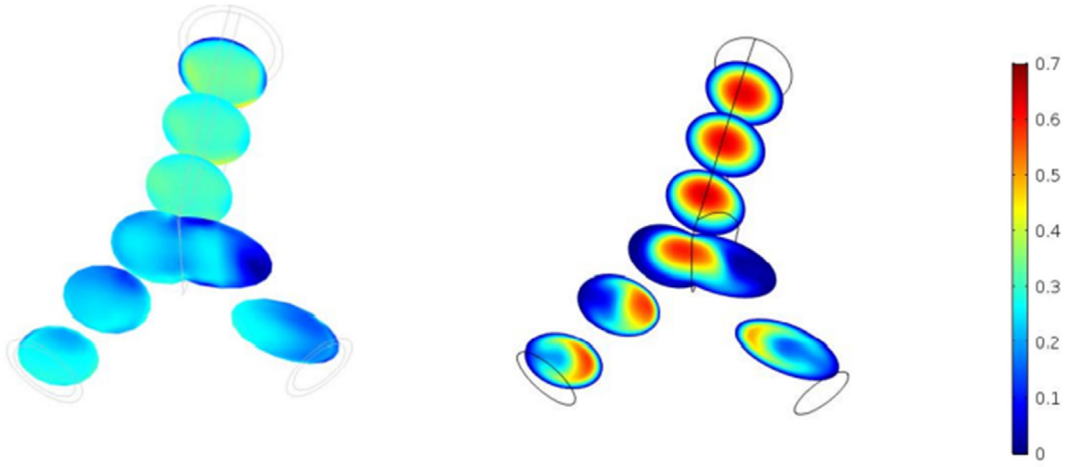


**Fig. 15** Velocity distribution at moment $t_2$ for viscosity 0.0035pa.s, right: rigid, left: flexible.

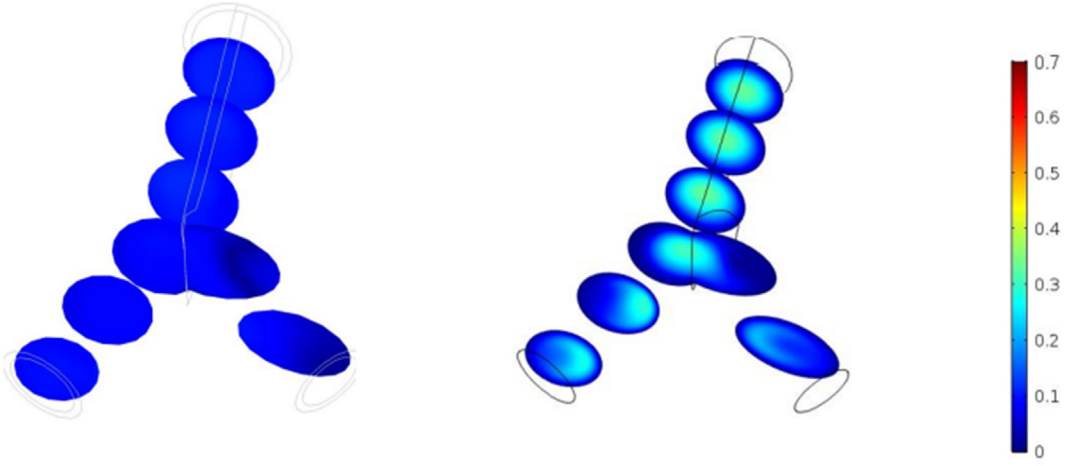


**Fig. 16** Velocity distribution at moment $t_3$ for viscosity 0.0035pa.s, right: rigid, left: flexible.

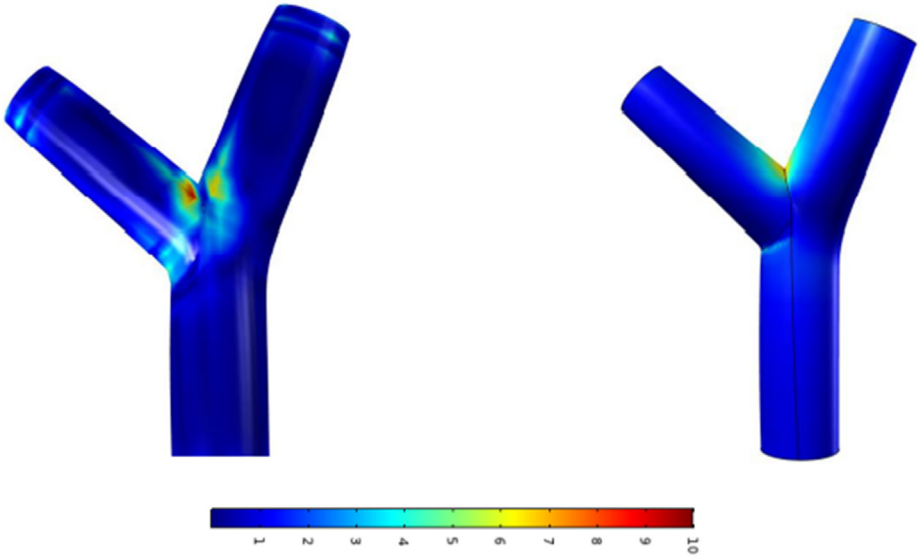


**Fig. 17** Shear stress distribution at moment $t_1$ for viscosity 0.0035pa.s, right: rigid, left: flexible.

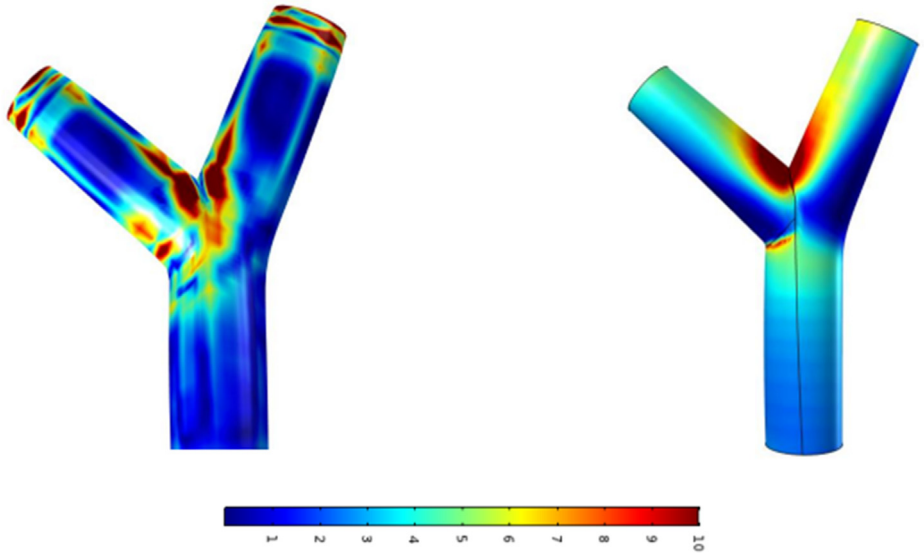


**Fig. 18** Shear stress distribution at moment $t_2$ for viscosity 0.0035pa.s, right: rigid, left: flexible.

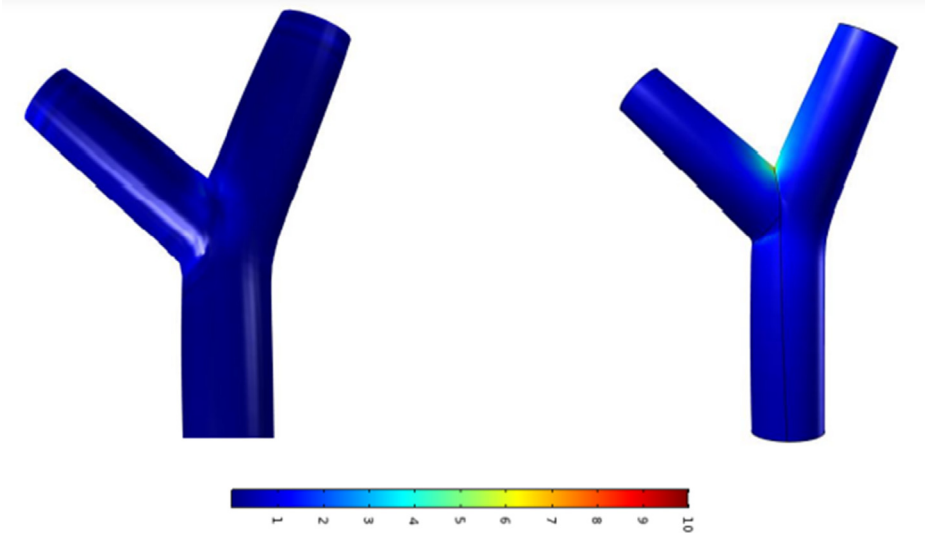


**Fig. 19** Shear stress distribution at moment $t_3$ for viscosity 0.0035pa.s, right: rigid, left: flexible.

Fig. 20 displays the flow velocity profile at the main entrance of the vessel. As you can see from the shape, the velocity is highest at the center of the vessel. The distance from the center to the walls is designed in such a way that the flow velocity gradually decreases until it reaches zero at the walls. At this moment, when the maximum flow velocity occurs at the entrance, the flow velocity in the center of the vessel increases as viscosity increases. The maximum flow velocity values for one heart cycle have been calculated for different viscosities (see Fig. 21). As shown in the figure, at low velocities, an increase in viscosity results in a decrease in the maximum flow velocity. By increasing the flow velocity at the entrance, the maximum flow velocity increased to its highest value. With increasing flow velocity, higher viscosities provide higher velocity values. At peak flow, the maximum flow velocity for viscosity 0.00924 (Pa.s) is 0.695 m/s and for viscosity 0.00289 (Pa.s) is 0.634 m/s. These values have increased by 6.8% and decreased by 2.53%, respectively, compared to the normal state.

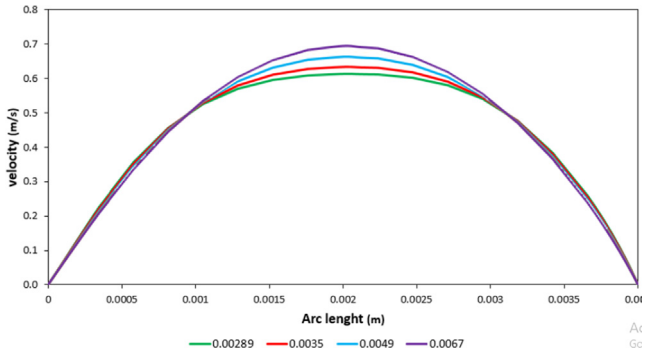


**Fig. 20** Flow velocity profile at the inlet boundary at the moment $t_2$.

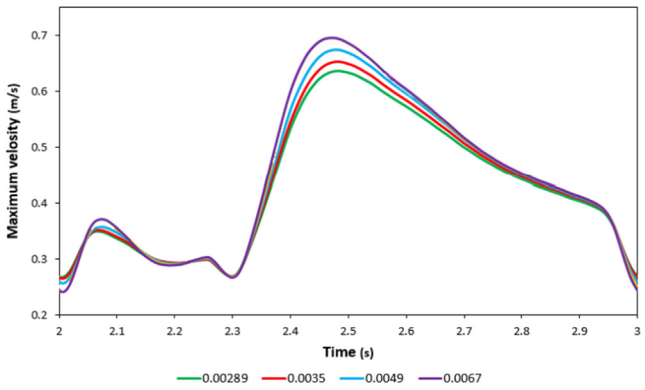


**Fig. 21** The maximum flow rate during one cycle of the heart for different viscosities.

The varying flow distribution results in a specific distribution of shear stress on the wall. To assess the overall impact of changes in viscosity on shear stress values, the average values of this parameter on the wall in Fig. 22 were analyzed. It is evident that an increase in viscosity leads to a remarkable rise in the average values of shear stress on the artery wall. Moreover, as the inlet flow velocity increases, the difference in shear stress values also increases for different viscosities. This difference reaches its maximum value at the peak velocity of the inlet flow.

Fig. 23 displays the highest values of shear stress during one heart cycle for various viscosities. It is well-established that high viscosities lead to a significant increase in shear stress values.

Fig. 24 illustrates the maximum Von Mises stress that occurs in the vessel wall. The Von Mises stress is calculated as follows:

$$\sigma_{von} = \sqrt{\frac{(\sigma_{11} - \sigma_{22})^2 + (\sigma_{22} - \sigma_{33})^2 + (\sigma_{11} - \sigma_{33})^2 + 6(\sigma_{12}^2 + \sigma_{23}^2 + \sigma_{31}^2)}{2}} \tag{10}$$

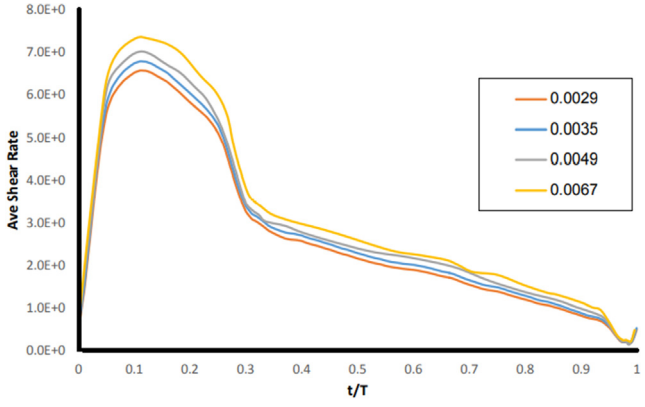


**Fig. 22** Average shear stress of the wall in one cycle of the heart for different viscosities.

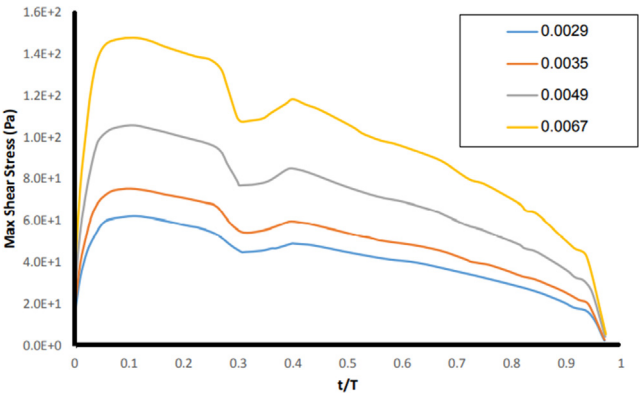


**Fig. 23** The maximum wall shear stress values in one cycle of the heart for different viscosities.

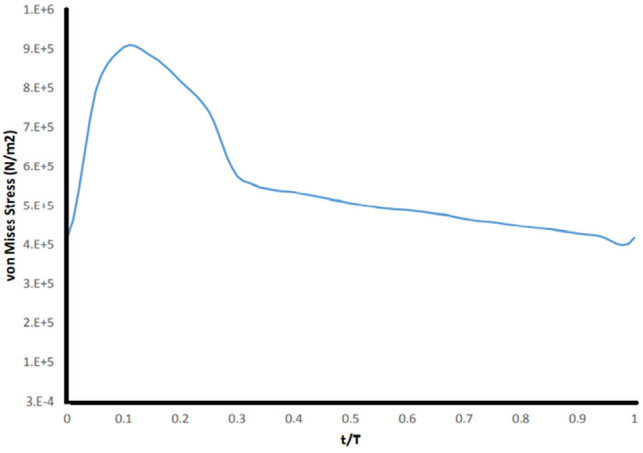


**Fig. 24** Maximum Von Mises stress in the vessel wall.

Von Mises stress provides an average estimate of the standard and shear stresses experienced by a solid element. As compressive stress is far more significant than shear stress, variations in viscosity have minimal impact on the Von Mises stress. Therefore, only the viscosity diagram for 0.0035 has been created.

Generally, changes in fluid viscosity have minimal impact on the shape and shear stress of the vessel wall, as normal stress (compression) typically dominates over shear stress. Hence, the flow parameters, particularly the hematocrit percentage of the blood, play a crucial role as they directly affect the viscosity values. This study highlights the significance of observing this parameter in predicting, diagnosing, and determining therapeutic measures for coronary arteries. Hence, such studies can greatly assist doctors in making informed decisions and adopting the best treatment approach by providing a thorough comprehension of the flow behavior in their patients' vessels. Thus, studies such as this can be crucial in aiding doctors to make informed decisions and choose the most effective treatment method by providing a comprehensive understanding of the flow behavior within their patients' vessels.

## 5. Conclusion

Cardiovascular diseases are unfortunately one of the leading causes of death in today's society. It is important to analyze blood flow in various parts of the circulatory system. The coronary artery is made up of four main arteries, and the left coronary artery is responsible for delivering blood to the heart muscle. This research utilizes computational fluid dynamics and finite element methods to investigate and analyze coronary vessels by studying changes in blood characteristics. The aim of this study is to analyze and model the flow of blood under different conditions of the coronary vessels, with a particular focus on the vessels on the left side. This is in response to changes in hematocrit, which can cause an increase or decrease in blood viscosity (measured in N.s/m2). In general, by applying condition flexibility for the vessel, it is possible to reduce pressure distribution on the wall when compared to the rigid model. When considering changes in viscosity, such as an increase from 0.0029 to 0.0067, this can lead to changes in the shear stress distribution on the wall. Specifically, this increase in blood viscosity causes maximum tension, resulting in the wall shear rising from 60 to 154 Pascal's, which is a 140% increase. Based on the current data, it appears that there is a high flow pressure in the artery, resulting in maximum relative pressure values of 6300 and 6450 Pascal's for the rigid and flexible models, respectively, at the separating joint of the bifurcation.

- Changes in fluid viscosity have little effect on the shape and shear stress of the vessel wall. This is because normal stress (compression) dominates over shear stress.
- In areas where the velocity of flow near the wall is high, the shear stress values on the wall are significant. Similarly, when the flow velocity reaches its lowest value, the shear stress values on the wall are minimal.
- Currently, the flow pressure in the artery is at very high values. As a result, in the separating joint of the bifurcation, the maximum relative pressure reaches 6300 and 6450 Pascal for the rigid and flexible models, respectively.
- Currently, the flow pressure in the artery is at very high values. As a result, in the separating joint of the bifurcation, the maximum relative pressure reaches 6300 and 6450 Pascal for the rigid and flexible models, respectively.

## Declaration of Competing Interest

The authors declare that they have no known competing financial interests or personal relationships that could have appeared to influence the work reported in this paper.

## Funding

Fund is not affiliated with this article.

## References

[1] S. Numata, K. Itatani, K. Kanda, K. Doi, S. Yamazaki, K. Morimoto, K. Manabe, K. Ikemoto, H. Yaku, Blood flow analysis of the aortic arch using computational fluid dynamics, Eur. J. Cardiothorac. Surg. 49 (6) (2016) 1578–1585.

[2] C.A. Taylor, C.A. Figueroa, Patient -specific modeling of cardiovascular mechanics, Annu. Rev. Biomed. Eng. 11 (1) (Aug. 2009) 109–134.

[3] X. Wang, X. Li, Computational simulation of aortic aneurysm using FSI method: influence of blood viscosity on aneurismal dynamic behaviors, Comput. Biol. Med. 41 (9) (2011) 812–821, https://doi.org/10.1016/j.compbiomed.2011.06.017.

[4] H.A. González, N.O. Moraga, On predicting unsteady non-Newtonian blood flow, Appl. Math Comput. 170 (2) (2005) 909–923.

[5] M. Silveira, R. Huebner, T.P. Navarro, Pulsatile blood flow in the thoracic aorta and aneurysm: a numerical simulation in CAD-built and patient-specific model, J. Braz. Soc. Mech. Sci. Eng. 39 (10) (2017) 3721–3728.

[6] A. Nardi, I. Avrahami, Approaches for treatment of aortic arch aneurysm, a numerical study, J. Biomech. 50 (2017) 158–165.

[7] A. Nardi, B. Even-Chen, I. Avrahami, Experimental and numerical study of the flow dynamics in treatment approaches for aortic arch aneurysms, in: K. Kirali (Ed.), Aortic Aneurysm, InTech, 2017.

[8] A.A. Basri et al, Numerical study of haemodynamics behaviour in normal and single stenosed renal artery using fluid-structure interaction, J. Adv. Res. Fluid Mech. Thermal Sci. 51 (1) (2018) 91–98.

[9] D. Meza, D.A. Rubenstein, W. Yin, A fluid–structure interaction model of the left coronary artery, J. Biomech. Eng. 140 (2018) 12.

[10] M. Bukač, S. Čanić, J. Tambača, Y. Wang, Fluid–structure interaction between pulsatile blood flow and a curved stented coronary artery on a beating heart: a four stent computational study, Comput. Methods Appl. Mech. Eng. 350 (2019) 679–700.

[11] M. Roustaei, M.R. Nikmaneshi, B. Firoozabadi, Simulation of Low Density Lipoprotein (LDL) permeation into multilayer coronary arterial wall: Interactive effects of wall shear stress and fluid-structure interaction in hypertension, J. Biomech. 67 (2018) 114–122.

[12] Y. Qiao, Y. Zeng, Y. Ding, J. Fan, K. Luo, T. Zhu, Numerical simulation of two-phase non-Newtonian blood flow with fluid-structure interaction in aortic dissection, Comput. Methods Biomech. Biomed. Eng. 22 (6) (2019) 620–630.

[13] S.S. Ardahaie, A.J. Amiri, A. Amouei, K.h. Hosseinzadeh, D.D. Ganji, Investigating the effect of adding nanoparticles to the blood flow in presence of magnetic field in a porous blood arterial, Inf. Med. Unlocked 10 (2018) 71–81.

[14] M. Alizadeh, D.D. Ganji, Heat transfer characteristics and optimization of the efficiency and thermal resistance of a finned thermosyphon, Appl. Therm. Eng. 183 (2021) 116136.

[15] J.-H. He, T.S. Amer, H.F. El-Kafly, A.A. Galal, Modelling of the rotational motion of 6-DOF rigid body according to the Bobylev-Steklov conditions, Results Phys. 35 (2022) 105391.

[16] W. Muhammad, A.P. Brahme, U. Ali, J. Hirsch, O. Engler, H. Aretz, J. Kang, R.K. Mishra, K. Inal, Bendability enhancement of an age-hardenable aluminum alloy: Part II—multiscale numerical modeling of shear banding and fracture, Mater. Sci. Eng. A 754 (2019) 161–177.

[17] M. Hatami, J. Zhou, D. Jing, in: Nanofluids and Mass Transfer, Elsevier, 2022, pp. 297–325.

[18] H. Behzadnia et al, Geometry optimization for a rectangular corrugated tube in supercritical water reactors (SCWRs) using alumina-water nanofluid as coolant, Energy 221 (2021) 119850.

[19] S.M. Mousazadeh, M.M. Shahmardan, T. Tavangar, K.h. Hosseinzadeh, D.D. Ganji, Numerical investigation on convective heat transfer over two heated wall-mounted cubes in tandem and staggered arrangement, Theor. Appl. Mech. Lett. 8 (3) (2018) 171–183.

[20] K.h. Hosseinzadeh, D.D. Ganji, F. Ommi, Effect of SiO2 super-hydrophobic coating and self-rewetting fluid on two phase closed thermosyphon heat transfer characteristics: an

experimental and numerical study, J. Mol. Liq. 315 (2020) 113748.
[21] B. Shaker, M. Gholinia, M. Pourfallah, D.D. Ganji, CFD analysis of Al2O3-syltherm oil Nanofluid on parabolic trough solar collector with a new flange-shaped turbulator model, Theor. Appl. Mech. Lett. 12 (2) (2022) 100323.
[22] M. Armin, M. Gholinia, M. Pourfallah, A.A. Ranjbar, Investigation of the fuel injection angle/time on combustion, energy, and emissions of a heavy-duty dual-fuel diesel engine with reactivity control compression ignition mode, Energy Rep. 7 (2021) 5239–5247.
[23] O. Khandouzi, M. Pourfallah, E. Yoosefirad, B. Shaker, M. Gholinia, S. Mouloodi, Evaluating and optimizing the geometry of thermal foundation pipes for the utilization of the geothermal energy: numerical simulation, J. Storage Mater. 37 (2021) 102464.
[24] H. Nabi, M. Pourfallah, M. Gholinia, O. Jahanian, "Increasing heat transfer in flat plate solar collectors using various forms of turbulence-inducing elements and CNTs-CuO hybrid nanofluids." Case Studies, Therm. Eng. 33 (2022) 101909.
[25] M. Javidan, M. Asgari, M. Gholinia, M. Nozari, A. Asgari, D. D. Ganji, Thermal energy storage inside the chamber with a brick wall using the phase change process of paraffinic materials: a numerical simulation, Theor. Appl. Mech. Lett. 12 (3) (2022) 100329.
[26] K.h. Hosseinzadeh et al, Effect of two different fins (longitudinal-tree like) and hybrid nano-particles (MoS2-TiO2) on solidification process in triplex latent heat thermal energy storage system, Alex. Eng. J. 60 (1) (2021) 1967–1979.
[27] A.G. Kanaris, A.D. Anastasiou, S.V. Paras, Modeling the effect of blood viscosity on hemodynamic factors in a small bifurcated artery, Chem. Eng. Sci. 71 (2012) 202–211.
[28] J. Dong, Z. Sun, K. Inthavong, J. Tu, Fluid–structure interaction analysis of the left coronary artery with variable angulation, Comput. Methods Biomech. Biomed. Eng. 18 (14) (2015) 1500–1508.
[29] P. Karmakar, A. Ali, S. Das, Circulation of blood loaded with trihybrid nanoparticles via electro-osmotic pumping in an eccentric endoscopic arterial canal, Int. Commun. Heat Mass Transfer 141 (2023) 106593.
[30] A. Ali, A. Barman, S. Das, EDL aspect in cilia-regulated bloodstream infused with hybridized nanoparticles via a microtube under a strong field of magnetic attraction, Thermal Sci. Eng. Progress 36 (2022) 101510.
[31] S. Das, P. Karmakar, A. Ali, Electrothermal blood streaming conveying hybridized nanoparticles in a non-uniform endoscopic conduit, Med. Biol. Eng. Compu. 60 (11) (2022) 3125–3151.
[32] A. Ali, A. Barman, S. Das, Electromagnetic phenomena in cilia actuated peristaltic transport of hybrid nano-blood with Jeffrey model through an artery sustaining regnant magnetic field, Waves Random Complex Media (2022) 1–32.
[33] A. Ali, R.N. Jana, S. Das, Significance of entropy generation and heat source: the case of peristaltic blood flow through a ciliated tube conveying Cu-Ag nanoparticles using Phan-Thien-Tanner model, Biomech. Model. Mechanobiol. 20 (6) (2021) 2393–2412.
[34] H. Bayissa Yadeta, S. Shaw, Magnetic drug targeting during casson blood flow in a microvessel: a caputo fractional model, J. Magn. Magn. Mater. 568 (2023) 170363.
[35] Kumar, N. Naresh, D. R. V. S. R. K. Sastry, and Sachin Shaw. "Irreversibility analysis of an unsteady micropolar CNT-blood nanofluid flow through a squeezing channel with activation energy-Application in drug delivery." Computer Methods and Programs in Biomedicine 226 (2022): 107156
[36] Alizadeh, As' ad, et al. "Numerical investigation of the effect of the turbulator geometry (disturber) on heat transfer in a channel with a square section." *Alexandria Engineering Journal* 69 (2023): 383-402.
[37] Abdollahi, Seyyed Amirreza, et al. "Investigating heat transfer and fluid flow betwixt parallel surfaces under the influence of hybrid nanofluid suction and injection with numerical analytical technique." *Alexandria Engineering Journal* 70 (2023): 423-439.
[38] A.K. Roy, S. Shaw, Shear augmented microvascular solute transport with a two-phase model: application in nanoparticle assisted drug delivery, Phys. Fluids 33 (3) (2021) 031904.
[39] S. Shaw, P.V.S.N. Murthy, Magnetic targeting in the impermeable microvessel with two-phase fluid model—Non-Newtonian characteristics of blood, Microvasc. Res. 80 (2) (2010) 209–220.
[40] S. Shaw, S.C. Pradhan, P.V.S.N. Murthy, "A FSI model on the Casson fluid flow through an elastic stenosed artery, Int. J. Fluid Mech. Res. 39 (6) (2012) 521–534.
[41] S. Somanath et al, Exploring the composite intentionality of 3D printers and makers in digital fabrication, Int. J. Des. 16 (3) (2022) 77–95.
[42] M. Garousi, S. Monazami Tabar, H. Mirazi, P. Asgari, P. Sabeghi, A. Salehi, A. Khaledi, M. Ghenaat Pisheh Sanani, H. K. Mirzahosseini, A global systematic review and meta-analysis on correlation between biofilm producers and non-biofilm producers with antibiotic resistance in Uropathogenic Escherichia coli, Microb. Pathog. 164 (2022) 105412.
[43] Nabizadeh, Mohammad, and Safa Jamali. "Life and death of colloidal bonds control the rate-dependent rheology of gels." Nature Communications 12.1 (2021): 4274.
[44] Hosseini, Saman, and Behrad Khamesee. "BIO-03 Design and control of a magnetically driven capsule-robot for endoscopy (bio-medical equipments I, technical program of oral presentations)." Proceedings of JSME-IIP/ASME-ISPS Joint Conference on Micromechatronics for Information and Precision Equipment: IIP/ISPS joint MIPE 2009. The Japan Society of Mechanical Engineers, 2009.
[45] L. Waite, J.M. Fine, Applied biofluid mechanics, McGraw-Hill, 2007.
[46] Bai, Jie, et al. "Numerical analysis and two-phase modeling of water Graphene Oxide nanofluid flow in the riser condensing tubes of the solar collector heat exchanger." *Sustainable Energy Technologies and Assessments* 53 (2022): 102408.A.E. Micah, et al., "Global investments in pandemic preparedness and COVID-19: development assistance and domestic spending on health the Lancet, Global Health between 1990 and 2026 11 (3) (2023) e385–e413.
[47] Mohammed, Ahmed Jameel, Masoud Muhammed Hassan, and Dler Hussein Kadir. "Improving classification performance for a novel imbalanced medical dataset using SMOTE method." *International Journal of Advanced Trends in Computer Science and Engineering* 9.3 (2020) 3161-3172.
[48] A. Karimipour, D. Toghraie, L.A. Abdulkareem, As'ad Alizadeh, M. Zarringhalam, A. Karimipour, Roll of stenosis severity, artery radius and blood fluid behavior on the flow velocity in the arteries: application in biomedical engineering, Med. Hypotheses 144 (2020) 109864.
[49] A. Alizadeh, A. Dadvand, Effects of deformability of RBCs on their dynamics and blood flow passing through a stenosed microvessel: an immersed boundary-lattice Boltzmann approach, Theor. Comput. Fluid Dyn. 32 (1) (2018) 91–107.